JNCI J Natl Cancer Inst (2017) 109(8): djw339

doi: 10.1093/jnci/djw339
First published online March 9, 2017
Article

ARTICLE

Effects of CTGF Blockade on Attenuation and Reversal of Radiation-Induced Pulmonary Fibrosis

Sebastian Bickelhaupt, Christian Erbel, Carmen Timke, Ute Wirkner, Monika Dadrich, Paul Flechsig, Alexandra Tietz, Johanna Pföhler, Wolfgang Gross, Peter Peschke, Line Hoeltgen, Hugo A. Katus, Hermann-Josef Gröne, Nils H. Nicolay, Rainer Saffrich, Jürgen Debus, Mark D. Sternlicht, Todd W. Seeley, Kenneth E. Lipson, Peter E. Huber

Affiliations of authors: Departments of Molecular and Radiation Oncology (SB, CT, UW, MD, PF, AT, JP, PP, LH, NJN, PEH) and Molecular Pathology (HJG), German Cancer Research Center, Heidelberg, Germany (DKFZ); Departments of Radiation Oncology (SB, CT, JP, NHN, JD, PEH), Cardiology (CE, HAK), Experimental Surgery (WG), Hematology and Oncology (RS), University Hospital Center, Heidelberg, Germany; Departments of Molecular Biology (MDS, TWS) and Drug Research (KEL), FibroGen, Inc., San Francisco, CA

Correspondence to: Peter Huber, MD, PhD, Department of Molecular and Radiation Oncology, German Cancer Research Center (DKFZ), 280 Im Neuenheimer Feld, Heidelberg 69120, Germany (e-mail: p.huber@dkfz.de).

Abstract

Background: Radiotherapy is a mainstay for the treatment of lung cancer that can induce pneumonitis or pulmonary fibrosis. The matricellular protein connective tissue growth factor (CTGF) is a central mediator of tissue remodeling.
Methods: A radiation-induced mouse model of pulmonary fibrosis was used to determine if transient administration of a human antibody to CTGF (FG-3019) started at different times before or after 20 Gy thoracic irradiation reduced acute and chronic radiation toxicity. Mice (25 mice/group; 10 mice/group in a confirmation study) were examined by computed tomography, histology, gene expression changes, and for survival. In vitro experiments were performed to directly study the interaction of CTGF blockade and radiation. All statistical tests were two-sided.
Results: Administration of FG-3019 prevented (~50%–80%) or reversed (~50%) lung remodeling, improved lung function, improved mouse health, and rescued mice from lethal irradiation ($P < .01$). Importantly, when antibody treatment was initiated at 16 weeks after thoracic irradiation, FG-3019 reversed established lung remodeling and restored lung function. CTGF blockade abrogated M2 polarized macrophage influx, normalized radiation-induced gene expression changes, and reduced myofibroblast abundance and Osteopontin expression.
Conclusion: These results indicate that blocking CTGF attenuates radiation-induced pulmonary remodeling and can reverse the process after initiation. CTGF has a central role in radiation-induced fibrogenesis, and FG-3019 may benefit patients with radiation-induced pulmonary fibrosis or patients with other forms or origin of chronic fibrotic diseases.

Radiotherapy is an important treatment for lung cancer. However, ionizing radiation induces acute and chronic side effects that limit the efficacy of radiotherapy (1–3). No treatments are approved for radiation-induced pulmonary fibrosis (4–6). The pathophysiologic events induced by radiation are similar to those that occur after other types of lung injury and idiopathic pulmonary fibrosis (IPF) (7,8). The common pathologic features of pulmonary fibrosis are dysregulated wound healing characterized by myofibroblast expansion and progressive deposition of extracellular matrix (ECM) (9–12). This aberrant tissue remodeling alters normal lung architecture, impairing gas exchange, lung function, and quality of life.

Received: October 20, 2015; **Revised:** October 9, 2016; **Accepted:** December 22, 2016

Key mediators of lung fibrosis have been identified, but a unified model of fibrogenesis has not been established (12,13). A number of treatment strategies have shown promising effects in rodent models of lung toxicity, including targeting free radical production (14), inflammatory cell recruitment, statins, and inhibitors of PDGF, VEGF, FGF, TGFß, Cox-2, integrin signaling (6,7,15–27), and targeting the TLR-4, CXCL12/CXCR4-axis, and NADPH-Oxidase 4 (28). The effectiveness of agents to halt fibrosis or reverse manifested lung remodeling in the clinic has yet to be investigated (29–33).

The matricellular protein connective tissue growth factor (CTGF) is a central mediator of tissue remodeling and fibrosis (34–37). CTGF has been reported to be an essential mediator for the fibrotic activity of TGFβ (38,39), but can also act independently of TGFβ. A role of CTGF expression has been described in mouse models of bleomycin-induced pulmonary fibrosis (40–43), and elevated CTGF expression was reported in patients with IPF (44–48).

Here we investigated whether blocking CTGF with FG-3019, a human monoclonal antibody that binds human and rodent CTGF, could attenuate and reverse pulmonary fibrosis after thoracic irradiation. The C57Bl/6 lung radiation model used is physiologically relevant because it exhibits a similar slow, progressive course and mechanisms characteristic of human fibrosis (1,49–51). Strong biphasic induction of CTGF expression in the lungs of irradiated C57Bl/6 mice has also been reported (50). FG-3019 was evaluated prior to observation of persistent lung remodeling (prevention) and after statistically significant lung remodeling was detectable (therapeutic intervention) (51).

Methods

Mouse Thorax Irradiation and CT Monitoring

All animal and cell procedures were approved by institutional and governmental authorities (DKFZ internal animal protection office; Regierungspraesidium Karlsruhe, Germany). Irradiation and monitoring of the six- to eight-week-old female C57Bl/6 mice (25 mice/group; 10 mice/group in a confirmatory study) were performed as previously described (15,52). Mice thoraces were irradiated with 20 Gy photons (6 MeV linac, dose rate 118 cGy/min, Siemens, Munich, Germany) (Supplementary Figure 1, available online). High-resolution computed tomography (HRCT; Aquilion, Toshiba, Minato, Japan) was analyzed for morphological and quantitative lung density. For the irradiation and CT procedures, mice were anesthetized by intraperitoneal application of 0.2 mg/kg Rompun (Bayer, Leverkusen, Germany) and 100 mg/kg ketamine 10% (Parke-Davis, Detroit, MI).

Antibody Treatment

FG-3019 is a human mAb and was administered (i.p., 10mg/kg, 3/week) for eight weeks starting two days before irradiation (pretreatment group), or two, 20, or 112 days (16 weeks) after irradiation (two-, 20- or 112-day groups). Control (nonirradiated) mice received FG-3019 or IgG for eight weeks beginning two days after experiment initiation. Placebo-treated mice received IgG for eight weeks beginning two days after irradiation. Antibodies were provided by Fibrogen, Inc. (San Francisco, CA) in histidine-buffered saline, pH 6.

Lung Histology

Histological analysis was performed as previously described (15,52). In brief, two to four mice/group were killed for histology on days scheduled for CT examination. Their lungs were fixed by intratracheal instillation of 4% formalin followed by overnight fixation, embedded in paraffin, sectioned at 5 μm, and stained with hematoxylin and eosin (H&E) or Sirius red for collagen deposition. Alpha-SMA staining was performed using Vector Elite Stain Kits (pk6101, Vector, Burlingame, CA) and an anti-αSMA-antibody (Abcam 5694-100; Abcam, Cambridge, UK). Macrophages were detected by a monoclonal rat antibody (Abcam, ab56297), and mastcells were stained by Giemsa (Dako, Hamburg, Germany). Visualization was performed using biotinylated secondary antibodies followed by an avidin-biotin peroxidase complex (Vectastain, PK6100; Vector, Burlingame, CA) and the chromogen 3,3'-diaminobenzidine (Vectastain, PK6100). Images were captured using a Nikon Eclipse E600 microscope equipped with a Nikon digital sight DS- U1 (Nikon Corp., Chiyoda, Tokyo, Japan) and analyzed with ImageJ Software Version 1.42q (National Institutes of Health, Bethesda, MD).

Health Status in Mice and Blood Gas Analysis

Blood was collected from the tail capillary of three mice/group, and oxygen content was measured on an ABL5 Radiometer blood gas analyzer (Radiometer GmbH, Willich, Germany). Mouse health was assessed semiquantitatively in at least three randomly chosen mice using a rank scale (0–3) assessing mobility, skin status, hunched back, breath rate, and weight.

Gene Expression in Mouse Lungs

RNA from two mice per group was quantified on one-color 4x44K mouse whole genome arrays (Agilent G4122F; Agilent, Santa Clara, CA). Array data were analyzed with Genespring GX (Agilent) software. Data were normalized to the median of eight nonirradiated control samples. Major expression patterns of probes altered substantially (≥twofold) and statistically significantly ($P < 0.01$) by irradiated (RT) relative to nonirradiated IgG controls or FG-3019 relative to RT alone were identified by principal components analysis. Cell type–specific origins of coordinately altered transcripts were confirmed using the mouse BioGPS database. All fold-change (Fc) values used for individual comparison between two groups met cutoffs for a greater than twofold increase or decrease in relative expression, calculated as the relative expression between the two groups. Data are available at ArrayExpress (accession number: E-TABM-1153).

In Vitro Assays

Primary isolated human endothelial and fibroblast cells (HUVEC, HDMEC), human pulmonary fibroblasts (HPF), normal human dermal fibroblasts (NHDF), primary human mesenchymal stem cells (MSC) (53), and human NSCLC A549 cells were treated with FG-3019 ± radiation. Clonogenic, cell proliferation, and Matrigel invasion/migration and proliferation coculture assays were performed. Immunoblots were probed with FG-3019, anti-αSMA, anti-collagen IV antibodies. Cell cycle and apoptosis assays using subG1 DNA and Caspase-3 were performed by FACS.

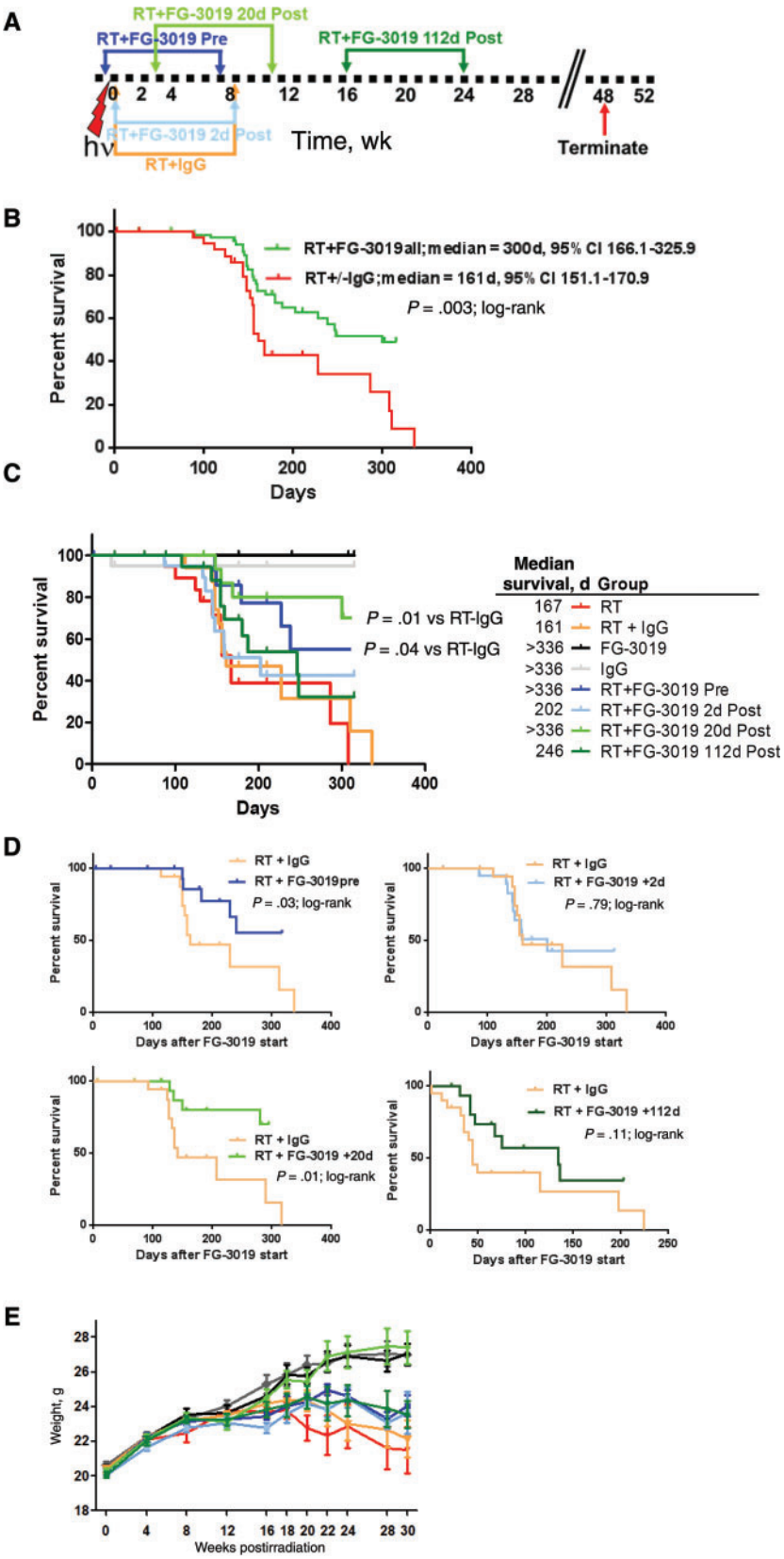

Figure 1. Influence of connective tissue growth factor blockade on mice survival and health status after lethal thorax irradiation. **A)** Experimental time course starting at the time of radiation. FG-3019 was administered to mice for eight weeks beginning two days before (RT+FG-3019 pre) irradiation or two days (RT+FG-3019 two days post), 20 days (RT+FG-3019 20 days post), or 112 days (16 weeks, RT+FG-3019 112 days post) after 20 Gy thorax irradiation. Four control groups were: Two groups were not irradiated but were exposed to a placebo antibody, human IgG (hIgG), or to FG-3019 (FG-3019) for the first eight weeks of the experiment. Two other groups were

Statistics

Mouse survival curves after thoracic irradiation and antibody treatments were calculated with the Kaplan-Meier method and analyzed using the log-rank test and the Cox proportional hazards model. The assumption of proportionality was verified by including time-dependent covariates in the Cox model and also by analyzing the Kaplan-Meier curves. Starting points for the log-rank test were the time of radiation or the time of FG-3019 start, as indicated. Mice killed for histological examination were censored. Other quantitative data are shown as mean values ± SD, as indicated. For analysis of differences between multiple groups, analysis of variance (ANOVA) was used, followed by the appropriate post hoc test. Expression data were analyzed using ANOVA with Bonferroni correction. Student's *t* test was used for parametric and Wilcoxon test for nonparametric variables. Correlation analyses were performed using Pearson correlation coefficient (PCC). All tests were two-tailed. *P* values of less than .05 were considered statistically significant. The Graphpad Prism (Version 6.0, Ja Jolla, CA) and Statistica (Statistica 5.0, Statsoft, Tulsa, OK) software packages were used.

For detailed methods, please refer to the Supplementary Materials and Methods (available online).

Results

Survival and Mouse Health after Lethal Thorax Irradiation

Thoracic irradiation without FG-3019 treatment was uniformly lethal and all mice died within 11 months, while transient FG-3019 treatment prolonged overall survival in a schedule-dependent manner (Figure 1, A–D). FG-3019 extended median survival of irradiated mice from 161 days (95% CI = 151.1 to 170.9) to 300 days (95% CI = 166.1 to 325.9; $P = .003$ for pooled, FG-3019-treated mice) (Figure 1B). The greatest survival benefit was achieved when FG-3019 treatment was initiated 20 days after irradiation with 70% survival at 48 weeks ($P = .01$) (Figure 1C). Initiation of FG-3019 two days before irradiation also increased survival ($P = .03$). The survival advantage from FG-3019 was present if data were analyzed from the time of radiotherapy or from the start of treatment (Figure 1D). FG-3019 was well tolerated and improved the health of irradiated mice (Figure 1E; Supplementary Table 1, available online). Mice in the 20-day group showed the greatest benefits and were most similar to nonirradiated control mice. Mice that started FG-3019 at 16 weeks after irradiation, when health deterioration was already evident, showed statistically significant and persistent health status improvement during the eight weeks of FG-3019 administration and after treatment was completed (Supplementary Table 1, available online). Irradiated mice (RT) and placebo-treated mice exhibited reduced weight vs controls ($P < .001$). FG-3019-treated groups attenuated the radiation-associated weight loss ($P = .008$ vs RT).

Computed Tomography of Lung Density Increases

A hallmark of lung fibrosis is increased tissue density, which is the basis of computed tomography (CT) analysis. Longitudinal CT monitoring demonstrated that the lung density of irradiated mice progressively increased after 12 weeks until 30 weeks (Figure 2, A–C). By eight weeks, CT morphology revealed high-density foci distributed throughout the lungs as typical signs of acute and subacute pneumonitis. By week 30, these dense foci fused to larger areas, indicative of chronic radiation damage and lung fibrosis. Reticular alterations and irregular septal thickening were typical CT findings characteristic of pulmonary fibrosis, consistent with histology. FG-3019 reduced CT signs of damage and lung densities. Early FG-3019 treatment attenuated the lung density increase by 42.8% (FG-3019 pre) and 46.5% (FG-3019 post day 2). FG-3019 initiation at day 20 almost completely prevented radiologically detectable lung damage, attenuated lung density increase by 83.3% (week 48 postirradiation), and yielded CT images comparable with nonirradiated control mice.

CT imaging also demonstrated that the lung density increase was reversible upon CTGF blockade: At 16 weeks, lung density was increased by 100 HU in irradiated mice without FG-3019 and continued to rise thereafter. FG-3019 administration starting at 16 weeks induced progressive lung density decreases that remained stable after treatment ceased (Figure 2C).

Lung and chest wall radiation-induced toxicity can alter the macroscopic structure and morphology of the thoracic scaffolding, leading to reduced lung size, mobility, and function. CT data revealed that FG-3019 also attenuated radiation-induced thorax shrinkage and cardiac hypertrophy (Supplementary Results and Supplementary Figure 2, A and B, available online).

Lung Function

In radiotherapy of lung cancer patients, a major side effect is worsening of lung function resulting in reduced blood oxygenation (3). We assessed gas exchange from tail capillary blood for oxygen partial pressure (paO_2). At 30 weeks, paO_2 levels were substantially below normal, indicating worsening of the oxygen status, while paO_2 values in the 20-day/16-week FG-3019 groups were in the normal range, indicating a positive effect on lung function (Figure 2D). In addition, the oxygen saturation data inversely correlated with lung densities measured by CT ($r^2 = 0.80$, $P < .001$) (Figure 2E). Thus, FG-3019 robustly improved function of irradiated lungs in a treatment- and schedule-sensitive manner, and CT lung density measurements were representative of lung function. For details, see the Supplementary Results (available online).

Lung and Cardiac Remodeling

Lung histology demonstrated progressive tissue remodeling after 12 weeks, with increasing alveolar septal thickness evident by 18 weeks reaching a plateau by 30 weeks (Figures 3, A–C; Supplementary Results and Supplementary Figure 3, available

Figure 1. Continued
irradiated and were untreated (RT) or treated with hIgG (RT+IgG), for eight weeks beginning two days after irradiation as a negative control (placebo-treated). **B and C)** Kaplan-Meier survival curves starting at the time of irradiation were based on 20 to 22 mice per group, with the mice killed for histological examination censored. **B)** Shows the pooled data of irradiated mice with no FG-3019 treatment vs the pooled data of the four irradiated groups treated with FG-3019 ($P = .002$, Cox regression). **C)** Shows the eight individual groups with median survival. If more than 50% of the mice at risk per group were still alive at the end of the experiment (48 weeks after irradiation), median survival is indicated as more than 336 days. **D)** Kaplan-Meier survival curves with the respective starting points at the time of FG-3019 treatment start. **E)** Body weights of mice, as a general measure of health status. **Bars** are mean ± SD. All statistical tests were two-sided. RT = irradiated.

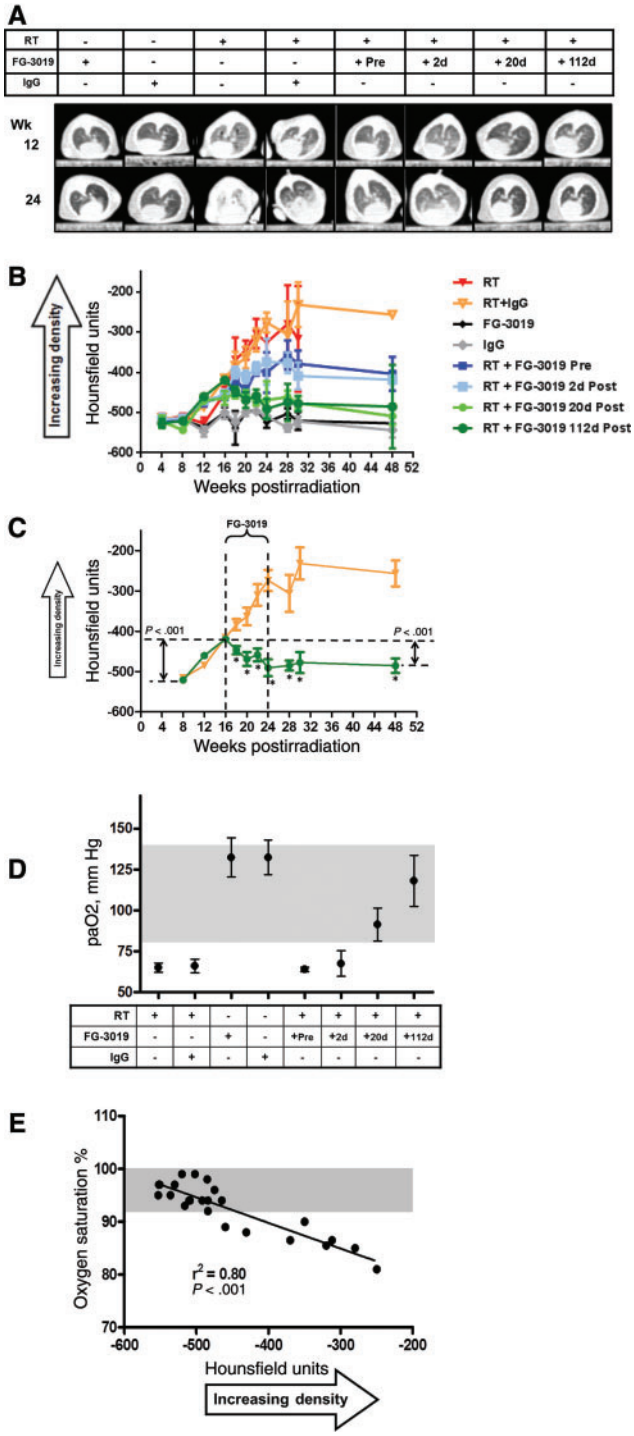

Figure 2. Lung density and function after thoracic irradiation. The lung density of mice in each group was analyzed radiologically by computed tomography (CT) and quantified in Hounsfield units (HU) at weeks 4, 8, 12, 16, 18, 20, 22, 24, 30, and 48 after irradiation. **A)** Representative computed tomography slices of mouse lungs at 12 and 24 weeks after irradiation. **White areas** represent high-density tissues (heart, bone, scar tissue**), black areas** represent air**, dark gray areas** are normal lung tissue (~ -520 HU), and **lighter gray areas** indicate increased density due to increased cellularity, edema, deposition of extracellular matrix proteins, and fibrosis. Lung fibrosis is characterized by diffuse bilateral areas of "ground glass" and intralobular reticular opacities. **B)** Quantitative lung density data derived from noninvasive computed tomography. All lung density data points in FG-3019-treated groups beginning 18 (20- and 112-day groups) or 20 (pretreatment and two-day groups) weeks after irradiation (RT) were statistically lower than in irradiated or placebo-treated groups ($P < .001$; two-way analysis of variance [ANOVA], Bonferroni post-test). Data are plotted as mean ± 95% confidence interval [CI]. **C)** Reversal of lung density in CT. The lung density of mice receiving FG-3019 beginning at 16 weeks after irradiation (RT+FG-3019 112 days post; **green circles**) compared with irradiated mice receiving placebo (RT+IgG; **orange triangles**, $P < .001$; two-way ANOVA, Bonferroni post-test). Data are plotted as mean ± 95% CI. **D)** Lung function by blood gas analysis. Blood from the mice tail capillaries analyzed for oxygen partial pressure (paO_2). The **gray area** indicates the normal range for paO_2, and data are shown as mean ± SD. **E)** Blood oxygen partial pressure data were converted to percent oxygen saturation and examined as a function of lung density based on radiological CT (Hounsfield units) data. The **shaded area** represents the normal range for oxygen saturation (>92%). The data were analyzed by linear regression analysis, and the best fit is shown by a **solid line**. All statistical tests were two-sided. CT = computed tomography; RT = irradiated.

online). Consistent late changes included alterations in the epithelium of bronchi and bronchioles including erosion, hyperplasia, and squamous metaplasia. By 30 weeks, extensive lung remodeling had occurred and morphometric analysis indicated that only approximately 30% of the alveolar area remained intact. Sirius Red staining revealed fibrotic patches of collagen, consistent with irradiation-induced fibrogenesis (Figure 3A). FG-3019 strongly reduced erosion, wall broadening, collagen deposition, and fibrosis in a schedule-dependent manner: The strongest beneficial effects of FG-3019 were seen in the 20-day group, which exhibited minimal change throughout the course of the experiment, and lungs that looked histologically normal at 30 weeks—more than two months after FG-3019 administration had halted.

In the 16-week group, septal thickening and pneumonitis were evident at 16 weeks, but lung remodeling was substantially resolved within two weeks of FG-3019 treatment and almost completely resolved by 24 weeks (Figure 3, B and D; Supplementary Results and Supplementary Figure 3, available online). Thus radiology and histology showed that FG-3019 robustly improved lung fibrosis–associated parameters and suggested that as little as two weeks of FG-3019 reversed delayed radiation-induced lung toxicity.

Furthermore, alpha-smooth muscle actin (αSMA) staining at 30 weeks showed that FG-3019 reduced irradiation-induced myofibroblast abundance (Figure 3E) as a potential mechanism for FG-3019's antifibrotic effects because myofibroblasts are involved in ECM deposition and lung remodeling in lung fibrosis (54). Likewise CTGF blockade between 16 and 18 weeks markedly reversed radiation-induced osteopontin/SPP1 mRNA and protein expression (Figure 3F), which is a potential biomarker for the development of pulmonary fibrosis (55–57).

Histology of the hearts revealed collagen deposits indicating mild myocardial fibrosis of both the right (RV) and left (LV) ventricle that were attenuated by FG-3019. Irradiation also increased the thickness of the right (RV) ventricle wall, which was attenuated by FG-3019 in the 20-day/16-week groups (Supplementary Results and Supplementary Figure 4, A and B, available online).

Acute Inflammation and Edema

FG-3019 pretreatment prevented leukocyte infiltration at day 2 (Figure 4A; Supplementary Results, available online), consistent with a report of CTGF affecting peripheral blood mononuclear cells (PBMC) recruitment (58,59). FG-3019 also suppressed acute septal thickening, a surrogate for interstitial edema (Figure 4A;

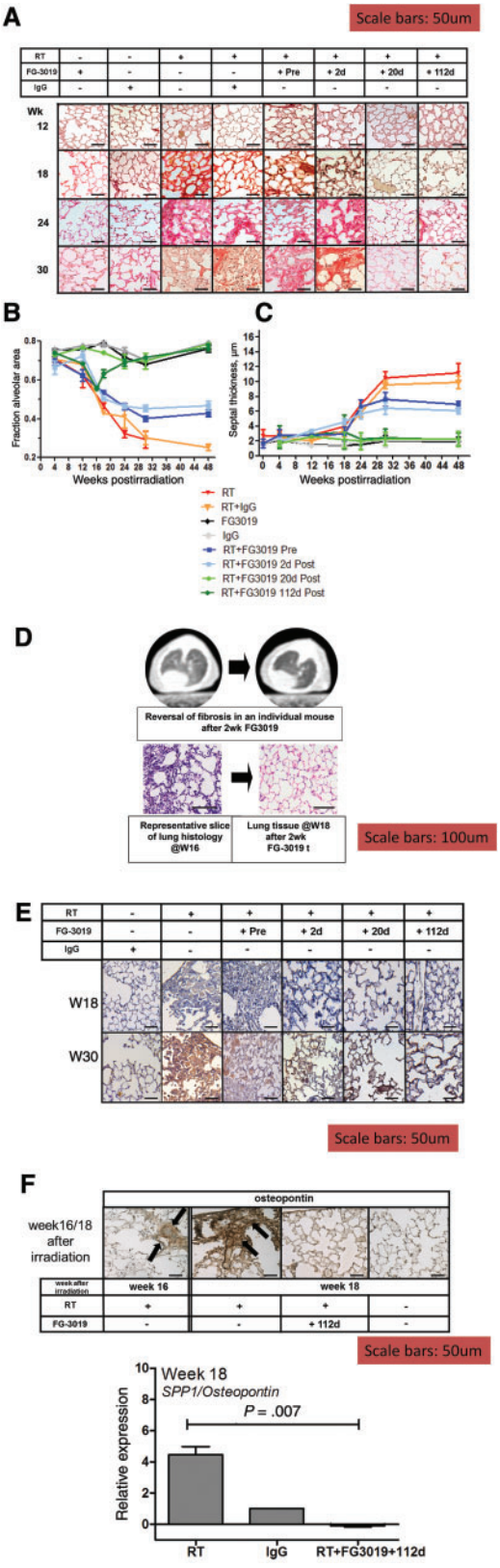

Figure 3. Pulmonary tissue remodeling after irradiation and connective tissue growth factor blockade. **A)** Sirius Red stained sections from mice in each group. **Scale bars** = 50 um. **B)** Alveolar area as a parameter for lung remodeling and lung function. Automated image analysis was performed on hematoxylin and eosin (H&E)–stained sections of lung tissue to determine alveolar area as a fraction of total area. **C)** Time course of alveolar septal thickness as a parameter for septal fibrosis. **D)** Reversal of lung density and remodeling in mice in the RT+FG-3019 112 days post group (16-week group). Longitudinal CT examinations in the same mouse (#454) at 16 and 18 weeks after irradiation (**top**). Representative H&E-stained slices from (different) mice taken at 16 and 18 weeks after irradiation (**bottom**). **Scale bars** = 100 um. **E)** Alpha smooth muscle actin staining. Representative immunohistochemistry (IHC) sections for α-SMA in lungs from mice showing effects of FG-3019 on irradiation-induced α-SMA. **Scale bars** = 50 um. **F)** Radiation-induced osteopontin expression after two weeks of FG-3019 at the protein and mRNA levels. **Top**: representative osteopontin IHC lung tissue in weeks 16 and 18. **Bottom**: osteopontin mRNA expression at 18 weeks after irradiation without or with two weeks of FG-3019 administration, compared with levels in lungs that were not irradiated (IgG). **Scale bars** = 50 um. All statistical tests were two-sided. RT = irradiation.

Supplementary Figure 5A, available online). This is relevant because edema allows extravascular fibrin to serve as a provisional matrix, promoting epithelial-to-mesenchymal transition (EMT) in response to stimuli like TGFβ (60) leading to formation of myofibroblasts. Together the data suggest a role for CTGF in radiation-induced acute edema and leukocyte influx (Supplementary Figure 7, available online).

Delayed Immune Response

The acute inflammation and edema spontaneously subsided by two weeks after irradiation. A subsequent inflammation phase reached a fourfold higher leucocyte peak at 18 to 20 weeks (Figure 4B; Supplementary Figure 5B, available online). FG-3019 reduced alveolar histiocytosis, characterized by sharp increases of macrophages and mast cells after 16 weeks (Figure 4, C and D). In the 16-week group, two weeks of FG-3019 reversed and prevented pulmonary leukocyte influx. Between 16 weeks and 18 weeks after irradiation, the relative percentage of macrophages increased disproportionally from 2.9% ± 0.29% to 34.1% ± 3.3% of all leukocytes ($P = .003$). FG-3019 reduced the macrophage influx and prevented this proportion shift, suggesting that macrophage influx drives fibrogenic lung remodeling in response to irradiation (Figure 4E).

Gene Expression Changes

Microarray analysis was performed to better understand reversal of the fibrotic process. Microarray expression profiling on 18-week lung samples (n = 2/group) showed that the expression of many transcripts was statistically significantly, substantially, and coordinately altered by radiation alone (Figure 5A). FG-3019 beginning 20 days or 16 weeks after irradiation produced a gene expression pattern resembling that of nonirradiated mice. This expression normalization in the 16-week therapeutic group suggested that inhibition of CTGF for only two weeks was sufficient to profoundly alter the biology of the remodeling lung. Analysis of individual genes showed that radiation increased transcripts associated with mesenchymal cell types and ECM remodeling, which were coordinately downregulated by FG-3019 (Figure 5B). Similarly regulated transcripts in the 20-day/16-week groups were characteristic of immune cell infiltration and/or have important roles in fibrosis, inflammation (61,62), immune cell recruitment (63), tissue destruction (64,65), myofibroblast stimulation, and collagen deposition, fibroblast survival (66), and EMT and ECM-deposition (Figure 5, B and C; Supplementary Table 2, available online) (67). The abrogation of leukocyte influx

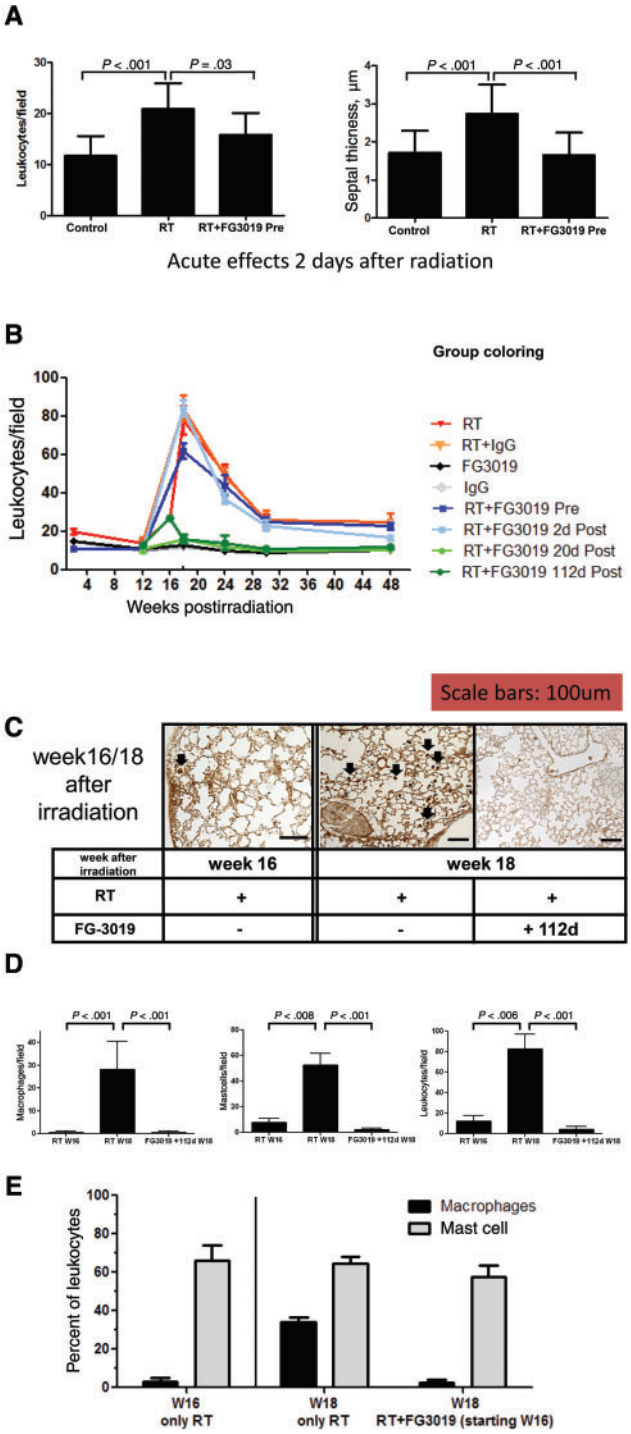

Figure 4. Acute and delayed pulmonary immune response to irradiation and connective tissue growth factor blockade. **A)** Quantification of acute pulmonary response: leukocyte infiltration (**left**) examined two days after irradiation. The number of leukocytes per high power field was counted, and the mean ± SD of 10 fields is plotted for nonirradiated mice (control), mice that were irradiated and untreated (RT), or mice that were administered FG-3019 for two days before irradiation (RT+FG-3019 pre). The mean ± SD septal thickness (**right**) are plotted for 50 septa (control) or 100 septa (RT and RT+FG-3019 pre). Statistical significance was determined by one-way analysis of variance (ANOVA) with a Tukey post-test. **B)** Time course of leucocyte infiltration in lungs showing a peak between weeks 16 and 24. Leukocyte infiltration was determined by counting the number of cells per high power field that exhibited a morphology characteristic of immune cells (ie, not epithelial or fibroblastic). The mean ± SD of 12 fields is plotted. Statistical significance for the 20-day and 16-week groups vs RT+IgG, $P < .01$, each. **C)** Histology of mouse lungs at 16 or 18 weeks after irradiation, without or with two weeks of treatment with FG-3019. **Black arrows** point to large cells with morphology characteristic of macrophages. **D)** Quantitation of leukocyte influx between weeks 16 and 18 revealed a statistically significant increase of total leukocytes, mast cells, and macrophages between weeks 16 and 18 in the RT group. **Bars** are mean ± SD of five immunohistochemistry fields from two mice; statistical significance was determined by one-way ANOVA with a Tukey post-test. **E)** The percentage of leukocytes in the lungs that were macrophages (**black bars**) or mast cells (**gray bars**) is shown at 16 weeks after irradiation and at 18 weeks after irradiation without or with two weeks of treatment with FG-3019. All statistical tests were two-sided. RT = irradiated.

by FG-3019 was reflected in the transcriptome by normalizing markers for mast cells and M2 polarized macrophages, but not M1 macrophages (Figure 5, B–D) (68,69). The expression data suggest that FG-3019 acted in a concerted manner rather than by blocking a single antifibrotic pathway (Supplementary Results and Supplementary Figures 5 and 6, available online).

Fibroblasts, Mesenchymal Stem Cells, and TGFβ-Stimulated EMT

In vitro, FG-3019 exhibited little toxicity in clonogenic survival and proliferation assays in primary human endothelial cells (HUVEC, HDMEC), fibroblasts (NHDF, HPF), and A549 lung cancer cells. (Figure 6, A and B). FG-3019 reduced constitutive (100 µg/mL: 68.3%, SD = 6.4%, $P = .007$; 30 µg/mL: 38.2%, SD = 7.8%, $P = .03$) and TGFβ-stimulated HPF migration (30 µg/mL: 58.1%, SD = 6.7%, $P = .01$) (Figure 6C). It attenuated TGFβ-stimulated differentiation or EMT with reduced expression of α-SMA and collagen IV protein in HPF and A549 cells (Figure 6D), and attenuated TGFβ induced epithelial-to-mesenchymal phenotype change (data not shown), supporting the hypothesis that CTGF blockade disrupts TGFβ-mediated fibrogenesis. FG-3019 did not alter the intrinsic cellular radiosensitivity of endothelial cells, fibroblasts, and A549 lung cancer cells (Figure 6, E–H), or human mesenchymal stem cells. It had only mild and subadditive antimigratory and antiproliferative effects when combined with radiation (Figure 6, I–K). FG-3019 did not alter the radiation-induced G2 cell cycle block and did not statistically significantly increase apoptosis of MSC (Figure 6, L and M). In a coculture proliferation model of human MSC with HPF or endothelial cells (HDMEC), irradiation of MSC, HPF, and HDMEC in the bottom compartment stimulated paracrine MSC and HPF proliferation in the upper compartment, which was inhibited by FG-3019 for HPF but not for MSC. For example, irradiation of MSC stimulated HPF proliferation by 1.9-fold (SD = 0.22-fold, $P = .02$), which was reduced by FG-3019 to 1.1-fold (SD = 0.13-fold, $P = .03$) (Figure 6N).

Discussion

Transient administration of FG-3019, a human monoclonal antibody to CTGF, attenuated radiation-induced lung remodeling in C57Bl/6 mice and reversed the process after it had initiated. All FG-3019-treated groups demonstrated benefit: Radiation-induced lung remodeling was attenuated, prevented, or reversed (as assessed by histology and longitudinal CT), and the overall health and lifespan of the mice were improved. When FG-3019 treatment started 20 days after the irradiation, most mice (70%) were rescued from death despite having received a lethal radiation dose.

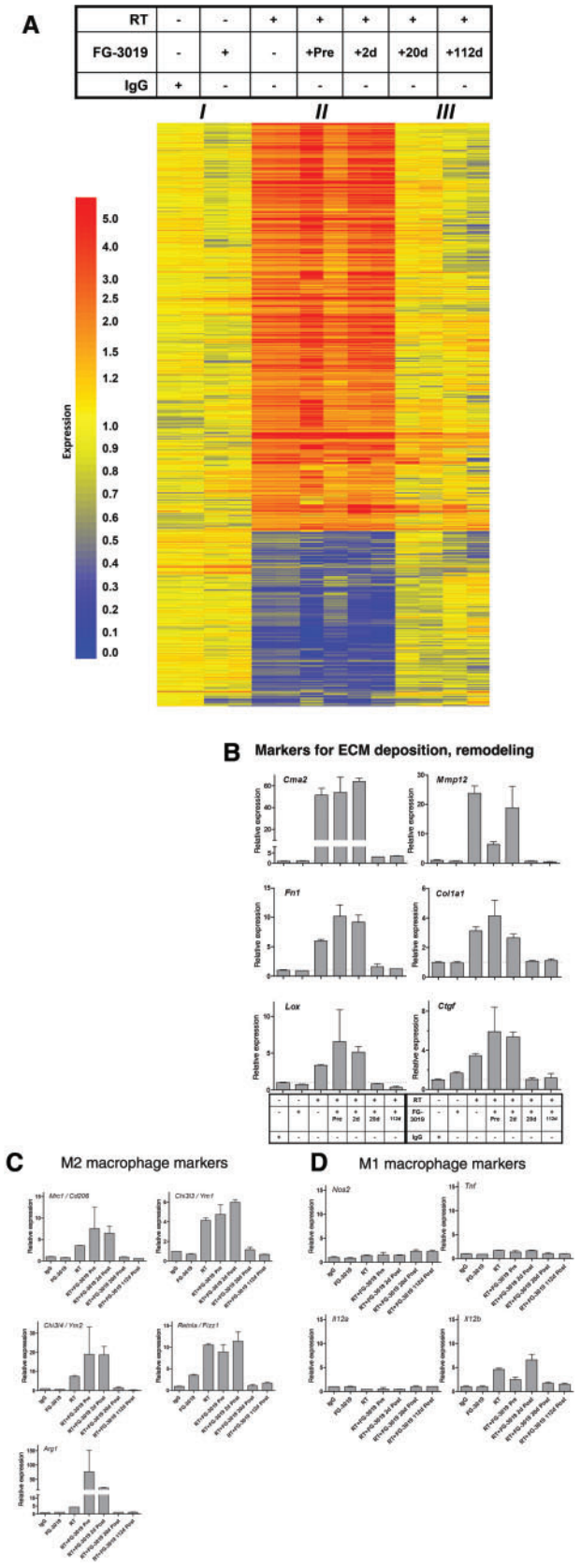

Figure 5. Radiation-induced gene expression changes in mouse lungs after connective tissue growth factor (CTGF) blockade. **A)** Clustering was performed on 938 probes (860 genes) altered at 18 weeks by RT vs IgG alone and/or by any FG-3019 treatment with RT vs RT alone (two mice per group). Relative expression is shown, representing two mice from each of the indicated treatment groups. Increased, unaltered, and diminished probes are indicated as **red**, **yellow**, and **blue**, respectively. The three main expression patterns are marked as: unirradiated controls (I), irradiated controls or irradiated-like (II), and irradiated but normalized (III). **B)** The expression of selected cell type–specific mRNA markers of mast cells (mast cell chymase 2, Cma2), macrophages (Mmp12, macrophage metalloelastase, matrix-metalloproteinase 12, a macrophage-specific MMP), and markers of myofibroblasts and extracellular matrix remodeling (CTGF, Ctgf; collagen 1α1, Col1a1; fibronectin, Fn1; lysyl oxidase, Lox) are shown as fold-change (mean ± SD) relative to their expression in nonirradiated, placebo-treated (IgG) mice. **C)** The expression of characteristic mRNA markers of M2 macrophages at week 18. Mrc1 (mannose receptor, C type 1), Ym1 (chitinase 3-like 3), Ym2 (chitinase 3-like 4), Fizz1 (found in inflammatory zone-1), Arg1 (arginase 1). **D)** The expression of characteristic mRNA markers of M1 macrophages at week 18. Nos2 (nitric oxide synthase), Tnf (tumor necrosis factor), and Il12a (interleukin 12a). Data are fold-change (mean ± SD) relative to their expression in nonirradiated, placebo-treated (IgG) mice. ECM = extracellular matrix; RT = irradiated.

CTGF may contribute to multiple aspects of the process of fibrosis. CTGF may directly modulate the formation of myofibroblasts by regulating transdifferentiation of fibroblasts or epithelial cells or indirectly contribute to myofibroblast formation by enabling edema leading to deposition of provisional matrix upon which epithelial cells undergo EMT. CTGF stimulates myofibroblasts to express chemokines and cytokines that recruit leukocytes and regulate their activity. CTGF also stimulates myofibroblasts to deposit and remodel ECM leading to changes in organ structure and function. Our data support this model by showing that FG-3019 reprogrammed fibrogenesis via normalization of the radiation-induced expression of genes involved in inflammation associated with M2 macrophage influx, EMT, myofibroblast activation, remodeling, and ECM deposition. Open questions remain with respect to radiation dose interdependence on the role of M2/M1 polarization changes that might affect inflammation type, vessel permeabilization, and tissue vascularization (70,71).

FG-3019 also normalized radiation-induced SMA and osteopontin protein and mRNA expression, suggesting a reduction of fibrotic disease activity because osteopontin has been implicated in fibrogenesis via ERK-dependent signaling and has been suggested as a biomarker for pulmonary fibrosis (72–74).

FG-3019 treatment starting 20 days after irradiation achieved the most profound benefits on lung structure and function. Treatment starting two days before/after irradiation, showed smaller benefits, suggesting that CTGF has an important role in radiation response between weeks 9 and 11 after irradiation, when early FG-3019 administration stopped, but was ongoing in the 20-day group.

FG-3019 two-day pretreatment resulted in longer survival than FG-3019 starting two days after irradiation despite the largely overlapping eight-week administration periods. One possible explanation is that FG-3019 pretreatment attenuated delayed responses to irradiation by preventing leucocyte influx and edema that allows extravascular fibrin to provide a provisional matrix upon which epithelial cells undergo EMT (60).

Therapeutic administration of FG-3019 reversed progressive lung remodeling, and lung densities decreased over the eight weeks of FG-3019 administration and remained stable without further treatment for another six months until the experiment was terminated. Similarly most radiologic, histologic, lung function, and health parameters reversed their disease progression. These data demonstrate that transient administration of FG-

ARTICLE

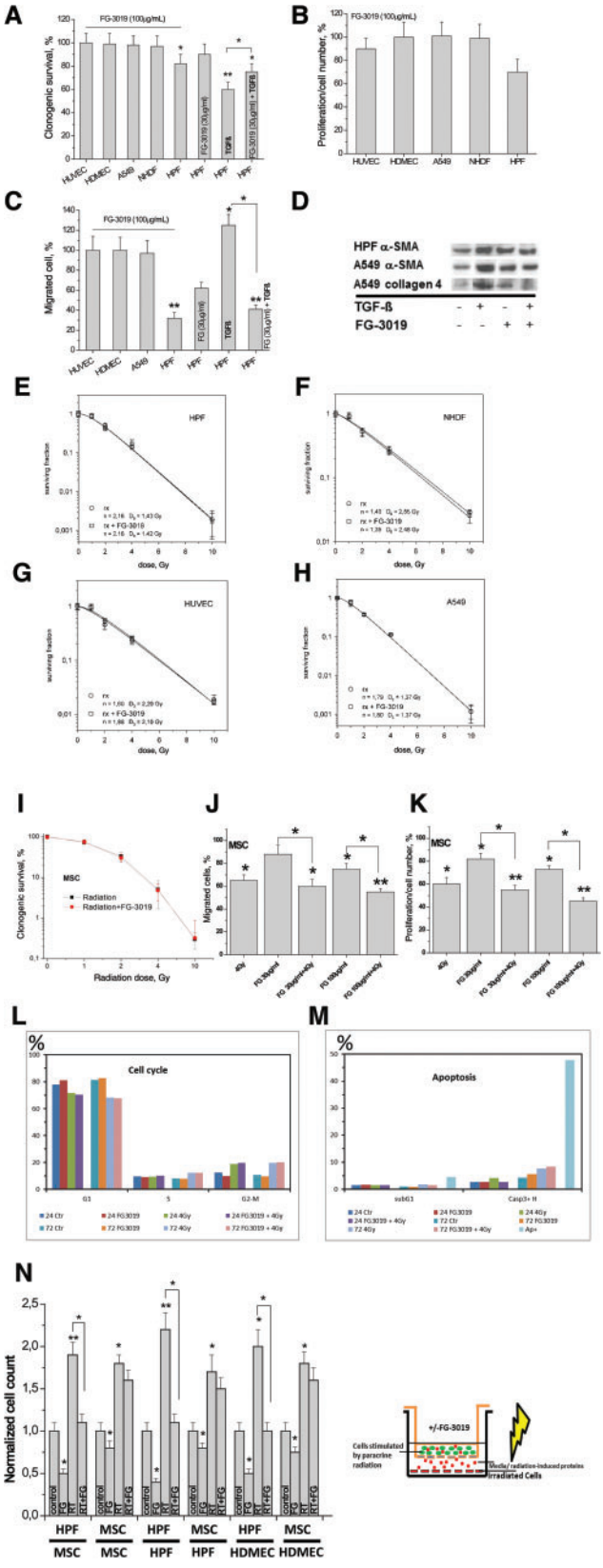

Figure 6. In vitro effects of FG-3019. **A)** Clonogenic survival, **(B)** proliferation, and **(C)** migration in vitro of human pulmonary fibroblasts (HPF, NHDF), endothelial cells (HUVEC, HDMEC), and lung cancer cells (A549) treated with FG-3019 alone or in combination with transforming growth factor ß1 (TGFβ1; 10 ng/mL). Each cell is normalized to its untreated control (100%). **Bars** indicate mean ± SD. **D)** Immunoblot, α-smooth muscle actin (α-SMA), or collagen 4 protein analysis in cells 48 hours after treatment with FG-3019 (30 µg/mL) and/or TGFβ1 (10 ng/mL). **E–I)** Clonogenic cell survival after radiation (rx) ± FG-3019 demonstrating no influence of FG-3019 on the intrinsic radiosensitivity in **(E)** HPF, **(F)** NHDF, **(G)** HUVEC, **(H)** A549, **(I)** mesenchymal stem cells (MSC). Two hours before irradiation cells were incubated with FG-3019 (30 µg/mL) and clonogenic, survival was determined. **Bars** are mean ± SD. Fit using the linear quadratic model with D0 and n values. **J)** Migration and **(K)** proliferation assay for MSC ± 4 Gy radiation, normalized to each untreated control (=100%). **Bars** are mean ± SD. **L)** FACS derived cell cycle distribution and **(M)** apoptosis quantification using subG1 and Caspase 3 detection 24 and 72 hours after 4 Gy ± FG-3019 at 30 µg/mL. **N)** Coculture proliferation assays were performed with HPF or MSC in the upper compartment of a Boyden chamber, with irradiated or nonirradiated HPF, MSC, or HDMEC in the lower compartment. For each set of cell pairs: Control (**first bar**) represents cells exposed to medium from nonirradiated cells in the absence of FG-3019; FG (**second bar**) represents cells treated with FG-3019 (30 µg/mL) and exposed to medium from nonirradiated cells; RT (irradiation, **third bar**) represents cells exposed to medium from irradiated cells in the absence of FG-3019; and RT+FG (**fourth bar**) represents cells treated with FG-3019 and exposed to medium from irradiated cells. Bars are mean ± SD. For all panels: *P < .05; **P < .01 (vs control or as indicated). Student's *t* test. All statistical tests were two-sided. HDMEC = endothelial cells; HPF = human pulmonary fibroblasts; HUVEC = human endothelial and fibroblast cells; NHDF = normal human dermal fibroblasts; TGFß = transforming growth factor ß1.

3019 had a durable effect and that the process of fibrosis could be reversed. The relatively modest improvement of survival in certain groups may have resulted from the early timing of the treatment or cumulative irreversible lung and/or cardiac toxicity already present at the time of treatment initiation (FG-3019 16 weeks).

Complex homeostatic processes like fibrogenesis are regulated by signaling networks controlled by positive and negative regulatory elements (51,75–77). Our data suggest that CTGF is a mediator of the shift from acute inflammation to a chronic fibrogenic inflammatory program, consistent with the hypothesis proposed by Kular (78) that CCN proteins are modulators of inflammation. Exposure to FG-3019 for only two weeks was sufficient to normalize the gene expression pattern and reprogram fibrotic processes.

In vitro, FG-3019 effects were modest, with no influence on the intrinsic radiosensitivity of cells. However, FG-3019 exhibited antimigratory and antiproliferative effects in fibroblasts/MSCs and attenuated TGFβ-stimulated differentiation, constituting mechanisms associated with fibrotic processes (79). The relative resistance of mesenchymal stem cells to FG-3019 and the preservation of MSC recruitment and paracrine stimulation upon radiation might be relevant for the putative regenerative function of MSC after radiation-induced lung damage (53,79,80)

Our study is not without limitations. We used only one eight-week FG-3019 administration scheme and one large single radiation dose, and neither dose dependence nor different radiation dose fractionations were examined. The complicated interdependence with heart damage also remains to be elucidated.

Overall, the data on blocking CTGF in a mouse model of radiation-induced lung toxicity are encouraging. The radiation-induced fibrosis model is a relevant trauma that initiates a series of events over almost one year that result in fibrosis and mimic what occurs in humans after irradiation. Transient administration of FG-3019 to irradiated mice prevented and reversed lung remodeling, preserved lung function, and provided a survival benefit. The monoclonal human antibody to CTGF may represent a promising new strategy to prevent, attenuate,

or reverse radiation-induced lung toxicity. The robustness and the magnitude of the beneficial effects provide translational relevance with potential for clinical transfer. FG-3019 is in clinical development in several indications, including idiopathic pulmonary fibrosis and pancreatic cancer. Our results indicate that CTGF plays an important role in radiation-induced lung toxicity and that blocking CTGF using FG-3019 could benefit patients undergoing radiotherapy in the thorax or may benefit patients with other forms of therapy-induced or idiopathic fibrotic diseases.

Funding

This work was supported in part by a grant from the German Radiation Research Consortium (Kompetenzverbund Strahlenforschung, KVSF, 03NUK004A,C of Bundesministerien fuer Bildung, Forschung und Umwelt, BMBF/BMU), FibroGen, Inc., and the NCT (Nationales Zentrum fuer Tumorerkrankungen), Heidelberg, Germany 3.0 Program on Radiotherapy and Immunology.

Notes

The study funders had no role in the design of the study; the collection, analysis, or interpretation of the data; the writing of the manuscript; or the decision to submit the manuscript for publication.

The authors thank Thuy Trinh, Sonevisay Sisombath, and Marina Szymbara for their excellent technical assistance.

SB designed and performed experiments, analyzed and interpreted data, and wrote the paper; CE performed experiments and analyzed data; CT performed experiments and analyzed data; UW performed experiments and analyzed data; AT performed experiments; JP performed experiments; WG designed and performed experiments; PP and LH performed experiments and interpreted and analyzed data; HAK analyzed and interpreted data; HJG analyzed and interpreted data; NHN analyzed and interpreted data; JD analyzed and interpreted data; MS analyzed and interpreted data; TS analyzed and interpreted data; KEL designed experiments, analyzed and interpreted data, and wrote the paper; PEH designed and performed experiments, analyzed and interpreted data, and wrote the paper. All authors contributed to manuscript writing and editing and approved the final version.

MS, TS, and KEL are employees of Fibrogen Inc., which kindly provided the anti-CTGF antibody FG-3019 for the study. PEH received grant support from Fibrogen Inc.

References

1. Rubin P, Constine LS, Fajardo LF, et al. Overview of late effects normal tissues (LENT) scoring system. *Radiother Oncol*. 1995;35(1):9–10.
2. Bentzen SM, Yarnold JR. Reports of unexpected late side effects of accelerated partial breast irradiation—radiobiological considerations. *Int J Radiat Oncol Biol Phys*. 2010;77(4):969–973.
3. McDonald S, Rubin P, Phillips TL, et al. Injury to the lung from cancer therapy: Clinical syndromes, measurable endpoints, and potential scoring systems. *Int J Radiat Oncol Biol Phys*. 1995;31(5):1187–1203.
4. Kwok E, Chan CK. Corticosteroids and azathioprine do not prevent radiation-induced lung injury. *Can Respir J*. 1998;5(3):211–214.
5. Johnston CJ, Manning C, Hernady E, et al. Effect of total body irradiation on late lung effects: Hidden dangers. *Int J Radiat Biol*. 2011;87(8):902–913.
6. Westbury CB, Yarnold JR. Radiation fibrosis—current clinical and therapeutic perspectives. *Clin Oncol*. 2012;24(10):657–672.
7. Flechsig P, Dadrich M, Bickelhaupt S, et al. LY2109761 attenuates radiation-induced pulmonary murine fibrosis via reversal of TGF-β and BMP-associated proinflammatory and proangiogenic signals. *Clin Cancer Res*. 2012;18(13):3616–3627.
8. Gross TJ, Hunninghake GW. Idiopathic pulmonary fibrosis. *New Engl J Med*. 2001;345(7):517–525.
9. Selman Ms, King JTE, Pardo A. Idiopathic pulmonary fibrosis: Prevailing and evolving hypotheses about its pathogenesis and implications for therapy. *Ann Intern Med*. 2001;134(2):136–151.
10. Strieter RM, Mehrad B. NEw mechanisms of pulmonary fibrosis. *CHEST J*. 2009;136(5):1364–1370.
11. Hardie WD, Glasser SW, Hagood JS. Emerging concepts in the pathogenesis of lung fibrosis. *Am J Pathol*. 2009;175(1):3–16.
12. Wilson MS, Wynn TA. Pulmonary fibrosis: Pathogenesis, etiology and regulation. *Mucosal Immunol*. 2009;2(2):103–121.
13. BS S, AM T. Role of the lysophospholipid mediators lysophosphatidic acid and sphingosine 1-phosphate in lung fibrosis. *Proc Am Thorac Soc*. 2012;9(3):102–110.
14. Epperly M, Epstein C, Travis E, et al. Decreased pulmonary radiation resistance of manganese superoxide dismutase (MnSOD)-deficient mice is corrected by human manganese superoxide dismutase-Plasmid/Liposome (SOD2-PL) intratracheal gene therapy. *Radiat Res*. 2000;154(4):365–374.
15. Abdollahi A, Li M, Ping G, et al. Inhibition of platelet-derived growth factor signaling attenuates pulmonary fibrosis. *J Exp Med*. 2005;201(6):925–935.
16. Anscher MS, Thrasher B, Zgonjanin L, et al. Small molecular inhibitor of transforming growth factor-β protects against development of radiation-induced lung injury. *Int J Radiat Oncol Biol Phys*. 2008;71(3):829–837.
17. Burdelya L, Krivokrysenko V, Tallant T, et al. An agonist of toll-like receptor 5 has radioprotective activity in mouse and primate models. *Science*. 2008;320(5873):226–230.
18. Gan L, Xue JX, Li X, et al. Blockade of lysophosphatidic acid receptors LPAR1/3 ameliorates lung fibrosis induced by irradiation. *Biochem Biophys Res Commun*. 2011;409(1):7–13.
19. Mathew B, Huang Y, Jacobson JR, et al. Simvastatin attenuates radiation-induced murine lung injury and dysregulated lung gene expression. *Am J Respir Cell Mol Biol*. 2011;44(3):415–422.
20. Rübe CE, Uthe D, Schmid KW, et al. Dose-dependent induction of transforming growth factor β (TGF-β) in the lung tissue of fibrosis-prone mice after thoracic irradiation. *Int J Radiat Oncol Biol Phys*. 2000;47(4):1033–1042.
21. Tsoutsou PG, Gourgoulianis KI, Petinaki E, et al. Cytokine levels in the sera of patients with idiopathic pulmonary fibrosis. *Respir Med*. 2006;100(5):938–945.
22. Williams J, Johnston C, Finkelstein J. Treatment for radiation-induced pulmonary late effects: Spoiled for choice or looking in the wrong direction? *Curr Drug Targets*. 2010;11(11):1386–1394.
23. Chaudhary NI, Roth GJ, Hilberg F, et al. Inhibition of PDGF, VEGF and FGF signalling attenuates fibrosis. *Eur Respir J*. 2007;29(5):976–985.
24. Daniels CE, Wilkes MC, Edens M, et al. Imatinib mesylate inhibits the profibrogenic activity of TGF-beta and prevents bleomycin-mediated lung fibrosis. *J Clin Invest*. 2004;114(9):1308–1316.
25. Anscher MS. Targeting the TGF-beta1 pathway to prevent normal tissue injury after cancer therapy. *Oncologist*. 2010;15(4):350–359.
26. Puthawala K, Hadjiangelis N, Jacoby SC, et al. Inhibition of integrin alpha(v)beta6, an activator of latent transforming growth factor-beta, prevents radiation-induced lung fibrosis. *Am J Respir Crit Care Med*. 2008;177(1):82–90.
27. Hunter NR, Valdecanas D, Liao Z, et al. Mitigation and treatment of radiation-induced thoracic injury with a cyclooxygenase-2 inhibitor, celecoxib. *Int J Radiat Oncol Biol Phys*. 2013;85(2):472–476.
28. Yang HZ, Wang JP, Mi S, et al. TLR4 activity is required in the resolution of pulmonary inflammation and fibrosis after acute and chronic lung injury. *Am J Pathol*. 2012;180(1):275–292.
29. Friedman SL, Sheppard D, Duffield JS, et al. Therapy for fibrotic diseases: Nearing the starting line. *Sci Transl Med*. 2013;5(167):161–167.
30. Wynn TA, Ramalingam TR. Mechanisms of fibrosis: therapeutic translation for fibrotic disease. *Nat Med*. 2012;18(7):1028–1040.
31. Kalash R, Epperly MW, Goff J, et al. Amelioration of radiation-induced pulmonary fibrosis by a water-soluble bifunctional sulfoxide radiation mitigator (MMS350). *Radiat Res*. 2013;180(5):474–490.
32. Jarman ER, Khambata VS, Cope C, et al. An inhibitor of NADPH oxidase-4 attenuates established pulmonary fibrosis in a rodent disease model. *Am J Respir Cell Mol Biol*. 2013;50(1):158–169.
33. Shu H-KG, Yoon Y, Hong S, et al. Inhibition of the CXCL12/CXCR4-axis as preventive therapy for radiation-induced pulmonary fibrosis. *PLoS One*. 2013;8(11):e79768.
34. Chen C-C, Lau LF. Functions and mechanisms of action of CCN matricellular proteins. *Int J Biochem Cell Biol*. 2009;41(4):771–783.
35. Abraham D. Connective tissue growth factor: Growth factor, matricellular organizer, fibrotic biomarker or molecular target for anti-fibrotic therapy in SSc? *Rheumatology*. 2008;47(suppl 5):8–9.
36. Lee CH, Shah B, Moioli EK, et al. CTGF directs fibroblast differentiation from human mesenchymal stem/stromal cells and defines connective tissue healing in a rodent injury model. *J Clin Invest*. 2010;120(9):3340–3349.
37. Lipson K, Wong C, Teng Y, et al. CTGF is a central mediator of tissue remodeling and fibrosis and its inhibition can reverse the process of fibrosis. *Fibrogenesis Tissue Repair*. 2012;5(suppl 1):S24.

ARTICLE

38. Grotendorst GR. Connective tissue growth factor: A mediator of TGF-β action on fibroblasts. *Cytokine Growth Factor Rev*. 1997;8(3):171–179.
39. Mori T, Kawara S, Shinozaki M, et al. Role and interaction of connective tissue growth factor with transforming growth factor-β in persistent fibrosis: A mouse fibrosis model. *J Cell Phys*. 1999;181(1):153–159.
40. Howell DCJ, Johns RH, Lasky JA, et al. Absence of proteinase-activated receptor-1 signaling affords protection from bleomycin-induced lung inflammation and fibrosis. *Am J Pathol*. 2005;166(5):1353–1365.
41. Joseph AL, Luis AO, Boihoang T, et al. Connective tissue growth factor mRNA expression is upregulated in bleomycin-induced lung fibrosis. *Am J Physiol*. 1998;275(2):365–371.
42. Bonniaud P, Martin G, Margetts PJ, et al. Connective tissue growth factor is crucial to inducing a profibrotic environment in "fibrosis-resistant" balb/c mouse lungs. *Am J Respir Cell Mol Biol*. 2004;31(5):510–516.
43. Wang Q, Usinger W, Nichols B, et al. Cooperative interaction of CTGF and TGF-beta in animal models of fibrotic disease. *Fibrogenesis Tissue Repair*. 2011;4(1):4.
44. Golec M, Lambers C, Hofbauer E, et al. Assessment of gene transcription demonstrates connection with the clinical course of idiopathic interstitial pneumonia. *Respiration*. 2008;76(3):261–269.
45. Ziesche R, Hofbauer E, Wittmann K, et al. A preliminary study of long-term treatment with interferon gamma-1b and low-dose prednisolone in patients with idiopathic pulmonary fibrosis. *New Engl J Med*. 1999;341(17):1264–1269.
46. Kono M, Nakamura Y, Suda T, et al. Plasma CCN2 (connective tissue growth factor; CTGF) is a potential biomarker in idiopathic pulmonary fibrosis (IPF). *Clinica Chimica Acta*. 2011;412(23–24):2211–2215.
47. Allen JT, Knight RA, Bloor CA, et al. Enhanced insulin-like growth factor binding protein–related protein 2 (connective tissue growth factor) expression in patients with idiopathic pulmonary fibrosis and pulmonary sarcoidosis. *Am J Respir Cell Mol Biol*. 1999;21(6):693–700.
48. Pan LH, Yamauchi K, Uzuki M, et al. Type II alveolar epithelial cells and interstitial fibroblasts express connective tissue growth factor in IPF. *Eur Respir J*. 2001;17(6):1220–1227.
49. Travis EL. The sequence of histological changes in mouse lungs after single doses of X-rays. *Int J Radiat Oncol Biol Phys*.1980;6(3):345–347.
50. Kalash R, Berhane H, Au J, et al. Differences in irradiated lung gene transcription between fibrosis-prone C57BL/6NHsd and fibrosis-resistant C3H/HeNHsd mice. *In Vivo*. 2014;28(2):147–171.
51. Walkin L, Herrick SE, Summers A, et al. The role of mouse strain differences in the susceptibility to fibrosis: A systematic review. *Fibrogenesis Tissue Repair*. 2013;6(1):18.
52. Plathow C, Li M, Gong P, et al. Computed tomography monitoring of radiation-induced lung fibrosis in mice. *Invest Radiol*. 2004;39(10):600–609.
53. Nicolay NH, Liang Y, Lopez Perez R, et al. Mesenchymal stem cells are resistant to carbon ion radiotherapy. *Oncotarget*. 2015;6(4):2076–2087.
54. Scotton CJ, Chambers RC. Molecular targets in pulmonary fibrosis*: The myofibroblast in focus. *CHEST J*. 2007;132(4):1311–1321.
55. Tsukui T, Ueha S, Abe J, et al. Qualitative rather than quantitative changes are hallmarks of fibroblasts in bleomycin-induced pulmonary fibrosis. *Am J Pathol*. 2013;183(3):758–773.
56. Schneider DJ, Lindsay JC, Zhou Y, et al. Adenosine and osteopontin contribute to the development of chronic obstructive pulmonary disease. *FASEB J*. 2010;24(1):70–80.
57. Vij R, Noth I. Peripheral blood biomarkers in idiopathic pulmonary fibrosis. *Transl Res*. 2012;159(4):218–227.
58. Cicha I, Yilmaz A, Klein M, et al. Connective tissue growth factor is overexpressed in complicated atherosclerotic plaques and induces mononuclear cell chemotaxis in vitro. *Arterioscler Thromb Vasc Biol*. 2005;25(5):1008–1013.
59. Wang X, McLennan SV, Allen TJ, et al. Regulation of pro-inflammatory and pro-fibrotic factors by CCN2/CTGF in H9c2 cardiomyocytes. *J Cell Commun Signal*. 2010;4(1):15–23.
60. Kim KK, Kugler MC, Wolters PJ, et al. Alveolar epithelial cell mesenchymal transition develops in vivo during pulmonary fibrosis and is regulated by the extracellular matrix. *Proc Natl Acad Sci U S A*. 2006;103(35):13180–13185.
61. Bani-Hani AH, Leslie JA, Asanuma H, et al. IL-18 neutralization ameliorates obstruction-induced epithelial-mesenchymal transition and renal fibrosis. *Kidney Int*. 2009;76(5):500–511.
62. Barnes TC, Anderson ME, Moots RJ. The many faces of interleukin-6: The role of il-6 in inflammation, vasculopathy, and fibrosis in systemic sclerosis. *Int J Rheumatol*. 2011;2011.
63. Szymczak WA, Deepe GS. The CCL7-CCL2-CCR2 axis regulates IL-4 production in lungs and fungal immunity. *J Immunol*. 2009;183(3):1964–1974.
64. Matute-Bello G, Wurfel MM, Lee JS, et al. Essential role of MMP-12 in fas-induced lung fibrosis. *Am J Respir Cell Mol Biol*. 2007;37(2):210–221.
65. Madala SK, Pesce JT, Ramalingam TR, et al. Matrix metalloproteinase 12-deficiency augments extracellular matrix degrading metalloproteinases and attenuates il-13–dependent fibrosis. *J Immunol*. 2010;184(7):3955–3963.
66. Liu X, Das AM, Seideman J, et al. The CC chemokine ligand 2 (CCL2) mediates fibroblast survival through IL-6. *Am J Respir Cell Mol Biol*. 2007;37(1):121–128.
67. Koenigshoff M, Kramer M, Balsara N, et al. WNT1-inducible signaling protein–1 mediates pulmonary fibrosis in mice and is upregulated in humans with idiopathic pulmonary fibrosis. *J Clin Invest*. 2009;119(4):772–787.
68. Gharib SA, Johnston LK, Huizar I, et al. MMP28 promotes macrophage polarization toward M2 cells and augments pulmonary fibrosis. *J Leukoc Biol*. 2014;95(1):9–18.
69. Novak ML, Koh TJ. Macrophage phenotypes during tissue repair. *J Leukoc Biol*. 2013;93(6):875–881.
70. Tsai CS, Chen FH, Wang CC, et al. Macrophages from irradiated tumors express higher levels of iNOS, arginase-I and COX-2, and promote tumor growth. *Int J Radiat Oncol Biol Phys*. 2007;68(2):499–507.
71. Klug F, Prakash H, Huber PE, et al. Low-dose irradiation programs macrophage differentiation to an iNOS(+)/M1 phenotype that orchestrates effective T cell immunotherapy. *Cancer Cell*. 2013;24(5):589–602.
72. Pardo A, Gibson K, Cisneros J, et al. Up-regulation and profibrotic role of osteopontin in human idiopathic pulmonary fibrosis. *PLoS Med*. 2005;2(9):e251.
73. Sabo-Attwood T, Ramos-Nino ME, Eugenia-Ariza M, et al. Osteopontin modulates inflammation, mucin production, and gene expression signatures after inhalation of asbestos in a murine model of fibrosis. *Am J Pathol*. 2011;178(5):1975–1985.
74. Kato A, Okura T, Hamada C, et al. Cell stress induces upregulation of osteopontin via the ERK pathway in type II alveolar epithelial cells. *PLoS One*. 2014;9(6):e100106.
75. Studer S, Kaminski N. Towards systems biology of human pulmonary fibrosis. *Proc Am Thorac Soc*. 2007;4(1):85–91.
76. Abdollahi A, Schwager C, Kleeff J, et al. Transcriptional network governing the angiogenic switch in human pancreatic cancer. *Proc Natl Acad Sci U S A*. 2007;104(31):12890–12895.
77. Hauser K, Abdollahi A, Huber PE. Inverse system perturbations as a new methodology for identifying transcriptomic signaling participants in balanced biological processes. *Cell Cycle*. 2009;8(17):2718–2722.
78. Kular L, Pakradouni J, Kitabgi P, et al. The CCN family: A new class of inflammation modulators? *Biochimie*. 2011;93(3):377–388.
79. Nicolay NH, Lopez Perez R, Debus J, et al. Mesenchymal stem cells—a new hope for radiotherapy-induced tissue damage? *Cancer Lett*. 2015;366(2):133–140.
80. Nicolay NH, Lopez Perez R, Saffrich R, et al. Radio-resistant mesenchymal stem cells: Mechanisms of resistance and potential implications for the clinic. *Oncotarget*. 2015;6(23):19366–19380.

ARTICLE